RSC Advances

PAPER

View Article Online
View Journal | View Issue

Cite this: *RSC Adv.*, 2024, **14**, 7877

High-performance biosensors based on angular plasmonic of a multilayer design: new materials for enhancing sensitivity of one-dimensional designs†

Hussein A. Elsayed, [ab] Suneet Kumar Awasthi, [c] Abdulkarem H. M. Almawgani, [d] Ahmed Mehaney, [*b] Yahya Ali Abdelrahman Ali,[e] Ahmad Alzahrani[df] and Ashour M. Ahmed [bg]

In this study, a theoretical examination is conducted to investigate the biosensing capabilities of different surface plasmon resonance (SPR) based hybrid multilayer structures, which are composed of two-dimensional (2D) materials. The transfer matrix formulation is implemented to calibrate the results of this study. A He–Ne laser of wavelength = 632.8 nm is used to simulate the results. Many permutations and combinations of layers of silver (Ag), aluminum oxynitride (AlON), and 2D materials were utilized to obtain the optimized structure. Ten dielectrics and twelve 2D materials were tested for a highly sensitive multilayer hybrid sensing design, which is composed of the prism (Ohara S-FPL53)/Ag/AlON/WS_2/AlON/sensing medium. The optimized biosensing design is capable of sensing and detecting analytes whose refractive variation is limited between 1.33 and 1.34. The maximum sensitivity, which is achieved by using the proposed design is 488.2° per RIU. Additionally, the quality factor, figure of merit, detection limit, and qualification limit values of the optimized design were also calculated to obtain a true picture of the sensing capabilities. The designing approach based on the multilayer hybrid SPR biosensors has the potential to develop various plasmonic biosensors that are related to food, chemical, and biomedical engineering fields.

Received 21st December 2023
Accepted 29th February 2024

DOI: 10.1039/d3ra08731j

rsc.li/rsc-advances

1. Introduction

The surface plasmon resonance (SPR) based optical sensing and detection technique is one of the most important and handy tools for real-time level-free detection of various biomedical and chemical applications, such as food protection, 24 hour medical care, enzymes, and drug diagnostics.[1–4] The SPR-based biosensing structures are highly sensitive because of their tremendous capability for identifying the minute fluctuations in the refractive index of the sensing medium due to the absorption of biomolecules of the order of 10^{-7}.[5] The incident transverse magnetic (TM) electromagnetic wave (EM) of a specific wavelength through the interface of a metal/dielectric slabs induces the free electrons of metal to oscillate collectively, which, in turn, start propagating along the interface due to the energy transfer, which is carried by the incident EM wave to free the electrons of metal surface.[6] This collective propagation of free electrons along the interface between the metal and dielectric is known as surface plasma waves (SPWs).[7] The coupling between SPWs and the evanescent wave, which results from phase matching, is a requirement for achieving the SPR conditions.[8] The fulfillment of this condition results in the resonant dip in the reflectance response of the structure[6–8] as the excitation of surface waves is not possible directly through a 3D beam. There are different excitation techniques, such as the Kretschmann configuration, in which, a prism is used for the excitation of surface plasmons, Otto configuration, fiber coupling, and greeting coupling schemes, which are used by researchers worldwide.[9] Amongst all these coupling schemes, Kretschmann configuration-based coupling scheme is the most popular coupling scheme for the excitation of evanescent waves by coating a nano-film of novel metal, such as (Au) and silver (Ag) on the prism surface through the TM polarized incident wave.[10] Gold is generally the ideal choice due to its capability to

[a]*Department of Physics, College of Science, University of Ha'il, Ha'il P.O. Box, 2440, Saudi Arabia*

[b]*Physics Department, Faculty of Science, Beni-Suef University, Beni-Suef, 62512, Egypt. E-mail: ahmed011236@science.bsu.edu.eg*

[c]*Department of Physics and Material Science and Engineering, Jaypee Institute of Information Technology, Noida, 201304, UP, India*

[d]*Electrical Engineering Department, College of Engineering, Najran University, Najran, Saudi Arabia*

[e]*Information Systems Department, College of Computer Sciences and Information Systems, Najran University, Najran, Saudi Arabia*

[f]*Scientific and Engineering Research Centre, Deanship of Scientific Research, Najran University, Najran, Saudi Arabia*

[g]*Physics Department, College of Science, Imam Mohammad Ibn Saud Islamic University (IMSIU), Riyadh, 11623, Saudi Arabia*

† Electronic supplementary information (ESI) available. See DOI: https://doi.org/10.1039/d3ra08731j

exhibit the plasmon resonance inside the visible wavelengths of the interacting electromagnetic waves.[11] However, hold is very expensive besides its relatively high metal absorption loss.

Despite its limitations, silver has directed significant attention to the fabrication of SPR-based sensors.[12] Silver has excellent conductivity, allowing for efficient transmission of electric current and minimizing energy losses, thereby making it ideal for various applications.[11–13] The evanescent waves can pass through the sensing medium and are ready for interaction with analytes available on the surface of the sensing medium. The minute change in the refractive index of the analyte available on the surface of the sensing medium could provide some changes in the propagation vector associated with an evanescent wave due to a shift in the phase-matching condition.[14] This change can be compensated by displacing the resonant dip, which is associated with the reflectance spectra of the structure and corresponds to the TM-polarized incident light. Additionally, the properties of the sensing medium in contact with the metal film can be observed by analyzing the changes in the intensity and angular position of the reflected light used to extract valuable information about the analyte. Furthermore, the SPR-sensing technology offers a remarkable capability to detect analytes across a wide concentration range from attomolar (aM) to nanomolar (nM) levels while analyzing various sample types, such as saliva, plasma, urine, and blood.[15]

Apart from several advantages of the SPR-based biosensing structures, such as portability, higher sensitivity, and dependability, some disadvantages can surface, such as a wider resonance dip, resulting in poor detection accuracy, a larger size biomolecule present in the sample may lower the sample concentration and, therefore, cannot be detected accurately by using the SPR biosensors.[16] Instead, large-range surface plasmon resonance (LRSPR) sensors can be employed to overcome these disadvantages.[17] In the LRSPR biosensing designs, a dielectric layer is sandwiched between the metal and semi-infinite prism. The requirement for achieving the LRSPR condition is to make the refractive indices of dielectric material and the aqueous solution poured on the surface of the sensing medium almost equal so that the evanescent field may penetrate deeper into the sensing medium to ensure the essential requirements of LRSPR configuration. Many studies were conducted on biosensors that are based on the phenomenon of LRSPR.[18–20]

In this regard, Wark *et al.* discussed how LRSPR-based biosensors can be used to investigate DNA hybridization. They have also mentioned the possible fabrication steps to design an LRSPR-based biosensing chip.[21] Pendry *et al.* proposed a theoretical design of biosensors based on the LRSPR phenomenon with a quality factor of 347 per RIU. The design is composed of five different layers of DBL, Mxene, FG, and sensing layers.[22] Arun *et al.* introduced a high-performance LRSPR sensor, which is composed of platinum diselenide and cytop layers of nanometer thickness.[23]

Recent scholarly research and development in the field of material science and engineering have provided us with an opportunity to discover new types of engineered materials, called 2D materials that enjoy excellent optical and electrical properties, such as tin selenide (SnSe), graphene oxide (GO), titanium disillicide ($TiSi_2$), graphene (G), antimonene (Sb), 2D (BlueP/WS_2), black phosphorus (BP), MXene ($Ti_3C_2T_x$), tungsten disulfide (WS_2), molybdenum diselenide ($MoSe_2$), tungsten diselenide (WSe_2), and molybdenum disulfide (MoS_2).[24–26] Today, these 2D materials are widely utilized by various research groups to design SPR-based biosensors, which are capable of detecting different biomolecules due to the robust interaction of biomolecules present in the analyte.[27,28] The fabrication of such materials is easier because they belong to the category of organic nanomaterials. Generally, the electrospinning fabrication technique is used for the fabrication of organic nanomaterials because it is a safe, swift, smooth, and cost-effective fabrication.[29] The properties of 2D materials listed above are promising and, thus, this study aims to investigate the viability of selecting the ideal 2D material for designing multilayer hybrid biosensors based on the SPR phenomenon.

In this work, the biosensors' capabilities of conventional and various nonconventional multilayer hybrid biosensing structures are investigated to construct the most sensitive SPR-based multilayer hybrid biosensing design Ohara S-FPL53 prism/Ag/AlON/WS_2/AlON/Sensing medium.

The organization of this study falls into five sections. Section 1 introduces the study. The mathematical framework of the study is presented in Section 2. Section 4 presents the results and provides a detailed discussion of the obtained results. Finally, the conclusion is presented in Section 5.

2. Mathematical framework

The transfer matrix formulation[30–36] is used for obtaining the reflectance of some conventional and nonconventional SPR-based plasmonic designs corresponding to transverse magnetic (TM) polarization cases. This formulation is preferred because it does not consider any kind of approximation. The nonconventional plasmonic designs are constructed of hybrid multilayers composed of metal, dielectric, and 2D material layers of thickness in nm order. Among all the seven structures, which are discussed in this paper, the proposed design of the best multilayer hybrid structure is displayed in Fig. 1. All the layers of the structure are fabricated on the Ohara S-FPL53 prism through the metallic layer of silver, as shown in Fig. 1. The top layer of the structure is composed of a semi-infinite sensing medium so that the analyte under investigation can be poured on the top surface of the structure. The presence of a metallic layer on the prism surface is used to excite the surface plasmons, which result from the total internal reflection as the incident angle becomes larger than the critical angle of the prism metal interface to produce the desired evanescent waves.

The geometry presented in Fig. 1 is assumed based on the design of the layers regarding the considered structures through z direction. Meanwhile, the refractive index and thickness of a given layer, p^{th} of the introduced structure are denoted by n_p and d_p, respectively. Then, a TM polarized light of wavelength = 632.8 nm from the He–Ne laser is allowed to couple into the proposed multilayer hybrid structure *via* Ohara S-FPL53 prism at an angle θ_I. One can easily connect the

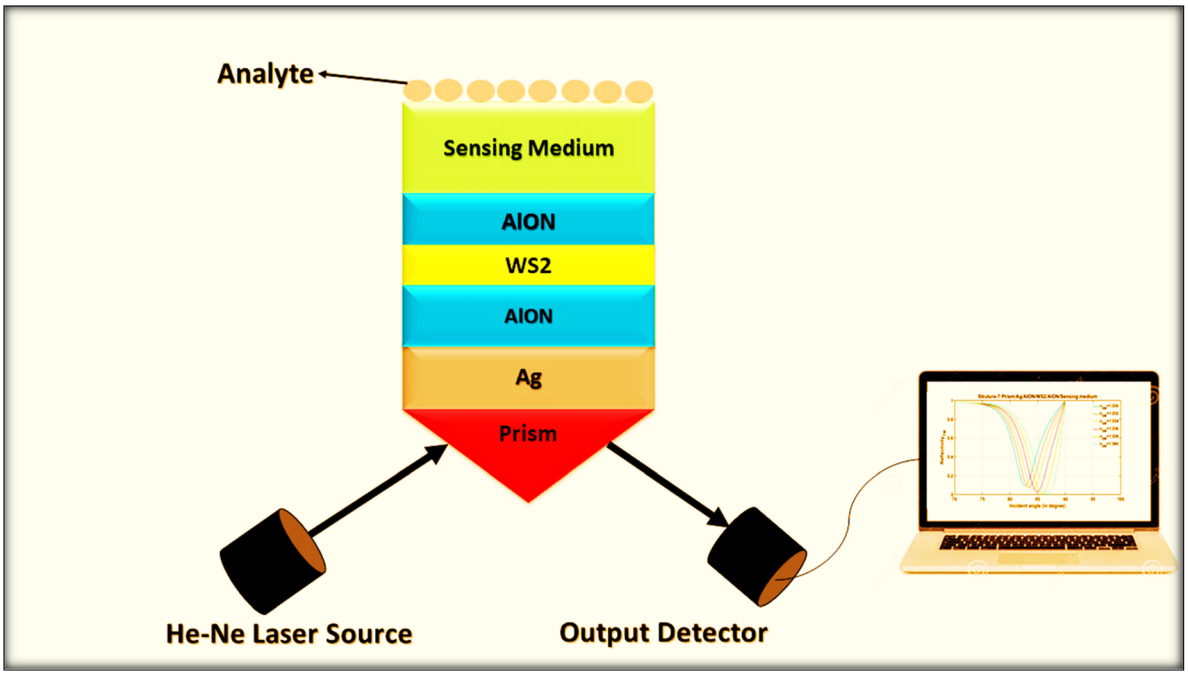

Fig. 1 A systematic view of optimized structure-7 composed of Ohara S-FPL53 prism/Ag/AlON/WS_2/AlON/sensing medium.

tangential components of electric and magnetic fields of light at the interface of the p^{th} layer of the structure through the transfer matrix formulation as follows:[37]

$$M_p = \begin{pmatrix} \cos\gamma_p & -\frac{i}{q_p}\sin\gamma_p \\ -iq_p\sin\gamma_p & \cos\gamma_p \end{pmatrix}, \quad (1)$$

Here, $q_p = \frac{\cos\theta_p}{n_p}$ and $\gamma_p = \frac{2\pi n_p d_p \cos\theta_p}{\lambda}$.

Snell's law can be used to connect the ray angle inside the p^{th} layer of the structure with the angle of incidence as $\cos\theta_p = \sqrt{1-\left(\frac{n_o\sin\theta_I}{n_p}\right)^2}$. Here, n_o represents the index of refractive of the incident medium. A similar approach is used to connect electric and magnetic fields vectors of light associated with each layer of the structure, including incident and exit medium as follows:[38]

$$\begin{pmatrix} E_1 \\ H_1 \end{pmatrix} = M^N \begin{pmatrix} E_{n+1} \\ H_{n+1} \end{pmatrix} = \begin{pmatrix} m_{11} & m_{12} \\ m_{21} & m_{22} \end{pmatrix} \begin{pmatrix} E_{n+1} \\ H_{n+1} \end{pmatrix} \quad (2)$$

Here, m_{11}, m_{12}, m_{21}, and m_{22} represent the transfer matrix elements of the whole structure. The reflection coefficient r_{TM} of the complete structure is given by ref. 33–38 as follows:

$$r_{TM} = \frac{(m_{11}q_0 + m_{12}q_sq_0) - (m_{22}q_s + m_{21})}{(m_{11}q_0 + m_{12}q_sq_0) + (m_{22}q_s + m_{21})} \quad (3)$$

Here, q_o and q_s indicate the incident ($z < 0$) and exit ($z > L$) ends of the structure of a total length L. As for the TM polarized wave $q_o = \frac{\cos\theta_I}{n_0}$ and $q_s = \frac{\cos\theta_s}{n_s}$. The notations n_0 and n_s show refractive indices of the incident and exit ends of the structure, respectively. As for the TM polarized wave, the reflectivity of the complete structure is given by ref. 33–38:

$$R_{TM} = |r_{TM}|^2. \quad (4)$$

3. Results and discussion

This section investigates the biosensing capabilities of different multilayer hybrid structures (MHSs) preliminary based on the phenomenon of surface plasma resonance. The biosensing capabilities of the proposed MHSs with the conventional SPR biosensors are investigated in this section. The details of all the SPR-based MHSs discussed in this study are illustrated in Table 1.

In all these biosensing structures, provisions are made in a way as to pour the analyte on the surface of the sensing medium, which is mounted on the top. In this study, the refractive index variation of the sample called analyte varies from 1.33 to 1.34 in steps of $\delta_n = 0.002$. The wavelength of 632.8 nm of incident light (He–Ne laser) has been presumed in the entire simulation work. To begin with, seven biosensing structures were selected based on conventional to hybrid SPR phenomena. The materials, which are used in designing the structures, are silver metal, a dielectric layer (DL), 2D material, and a sensing medium. To design all the structures, the Ohara S-FPL53 prism of the refractive index $n_{prism} = 1.43777$ is used as a substrate. The substrate is a semi-infinite thickness, which may vary from 1.5 cm to 2.5 cm.[39] A greater thickness of the substrate may increase the scattering losses. One of the structural designs, which is composed of metal, dielectric, 2D

Table 1 Details of the various categories of SPR-based biosensing structures

Structural details	Stacking of layers
Structure-1 (conventional SPR design)	Prism/Ag/sensing medium
Structure-2	Prism/Ag/DL/sensing medium
Structure-3	Prism/Ag/DL/2D/sensing medium
Structure-4	Prism/2D/DL/Ag/DL/sensing medium
Structure-5	Prism/DL/Ag/DL/2D/sensing medium
Structure-6	Prism/DL/2D/DL/Ag/sensing medium
Structure-7	Prism/Ag/DL/2D/DL/sensing medium

material, and sensing medium fabricated on Ohara S-FPL53 prism substrate is depicted in Fig. 1. In all the proposed plasmonic structures, the desired evanescent waves are created at the prism metal interface to excite surface plasmons by allowing the incident light to be incident on the structure at an angle that is greater than the critical angle so that the phenomenon of total internal reflection is executed. The coupling between the horizontal component of the wave vector of incident light and surface plasma polaritons (SPPs) of propagating wave vectors can be assisted by the prism in the SPR-based structures. The common structural parameters, which rely on the architecture of different SPR designs, are given in Table 2.

Next, the effect of change in the refractive index of the analyte from 1.33 to 1.34 on the reflectivity of all seven SPR designs has been examined. This change in the refractive index of the sensing medium appears in the form of a change in the resonance angle ($\Delta\theta_R$) of the resonant peak, which appears in the reflectivity *versus* the incident angle plot. The transfer matrix method is used to carry out simulations that are extracted from MATLAB computational software. The transfer matrix method is suitable because approximations are not used. The reflectivity spectra of the structures that are composed of Prism/Ag/sensing medium and Prism/Ag/DL/sensing medium are plotted in Fig. 2 and 3, respectively.

After pouring the analyte of the refractive index 1.33 on the surface of the sensing medium of SPR sensor-prism/Ag/sensing medium, a resonant dip of reflectivity of 38.94% is obtained at an angle of 78.27° in the reflectance spectra, as shown in Fig. 2. Next, the analyte of refractive index 1.34 is poured into the structure through an inlet valve to observe the effect of this change both on the position and reflection intensity of the resonance dip. This change in the refractive index of the analyte results in the shift in the position of the resonant dip from 76.35° to 78.27°, corresponding to the total change of 1.92° in the angular position of the resonant dip. Moreover, the increase in the refractive index of the sample also reduces the reflection intensity of the resonant dip, as demonstrated in Fig. 2. Actually, the appearance of this resonant dip is strongly associated with the total internal reflection (TIR) besides the coupling between the evanescent wave and the wave vector of surface plasmon.[2–4,6] When light travels at an angle greater than the critical angle from the prism to Ag's layer, TIR is expected to occur. Thus, a little portion of the incident electromagnetic waves is confined through Ag's layer as an evanescent wave.[6] Then, the excitation of SPR is introduced due to coupling between the confined evanescent wave and the surface plasmon resonance as a result of the matching between the wave vector of the incident electromagnetic wave and that of the surface plasmon.[2–6] Interestingly, the resonant dip appears within the reflectance spectrum due to the excitation of SPR.[5,6] Then, its position is shifted towards a new angle as the refractive index of the analyte changes due to the change in the optical path length of the incident light as shown in Fig. 2.

After that, an investigation has been carried out regarding how the insertion of an additional layer of dielectric material of refractive index 1.6 and thickness of 3 nm between the Ag layer and semi-infinite sensing medium of structure-1 can improve the change in the position of the resonant dip due to the change in the refractive index of analyte from 1.33 to 1.34. For this purpose, the reflectivity spectra of a modified structure composed of prism/Ag/DL/sensing medium are plotted, as shown in Fig. 3.

It is obvious from Fig. 3 that the presence of an additional dielectric layer in structure-2 enhances the transformation of the incident light, corresponding to TM polarization at the resonance angle into surface plasmons due to the energy reduction associated with resonance dip.[6] This enhancement of surface plasmons can be visualized by observing the decrease in the energy, which is associated with resonance dips, corresponding to the samples of refractive indices 1.33 and 1.34

Table 2 The refractive index and thickness values of different material layers at a wavelength of 632.8 nm fabricated on a prism substrate, depend upon the architecture of various SPR designs

Material details	Refractive index values	Thickness	Reference
Ohara S-FPL53 prism	1.43777	1.5 cm to 2.5 cm	39
Silver (Ag)	0.05626 + 4.2776i	40 nm	40
BlueP/WS_2	2.48 + 0.17i	0.75 nm	41
Sensing medium	1.33 to 1.34, $\delta_n = 0.002$	300 nm	—
Dielectric layer (DL)	1.6	3 nm	—

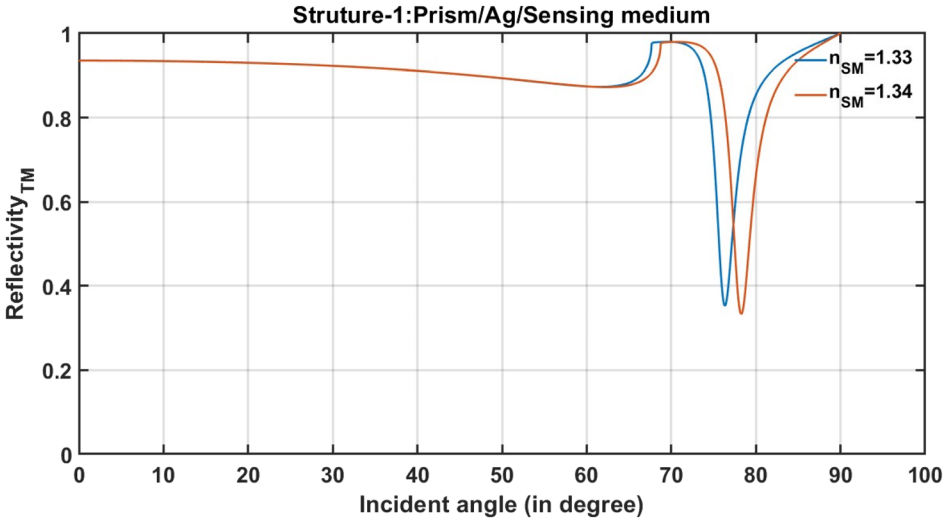

Fig. 2 The incident angle-dependent reflectivity of the conventional SPR structure (prism/Ag/sensing medium).

positioned at resonance angles 77.37° and 79.44°, respectively in the reflectance spectra, as shown in Fig. 3. Similarly, the change in the position of the resonant dip due to a change in the refractive index of the analyte from 1.33 to 1.34 of the remaining structures, *i.e.*, structure-3 to structure-7 is examined, as illustrated in Table 1. In all these structures, the stacking of the layers has been made by considering various permutations and combinations of different layers of metal, dielectric and 2D material, as per the details mentioned in Table 2. After designing these structures, the change in the position of the resonant dip due to a change in the refractive index of the analyte from 1.33 to 1.34 is examined by studying their respective reflectance spectra. The change in the position of the resonant dip due to the change in the refractive index of the analyte from 1.33 to 1.34 of each structure studied in this work is summarized in Table 3.

After comparing the shift in the position of resonant dips of the respective structures due to the change in the refractive index of analyte poured into the surface of the sensing medium of all seven structures separately, it was found that structure-7 possesses a maximum shift of 2.50° in the position of a resonant dip towards the higher side of incidence angle due to the change in the refractive index values of analyte from 1.33 to 1.34, as illustrated in Table 3. Thus, the architecture of structure-7 is the most suitable for investigating the samples whose refractive index variation is limited between 1.33 to 1.34. The efforts were further extended to increase the shift in the resonant dip due to the change in the refractive index of the analyte from 1.33 to 1.34. This idea has been implemented by considering various types of 2D materials of different thicknesses in the design of structure-7 and keeping other structural parameters constant, as per the provided data in Table 2.

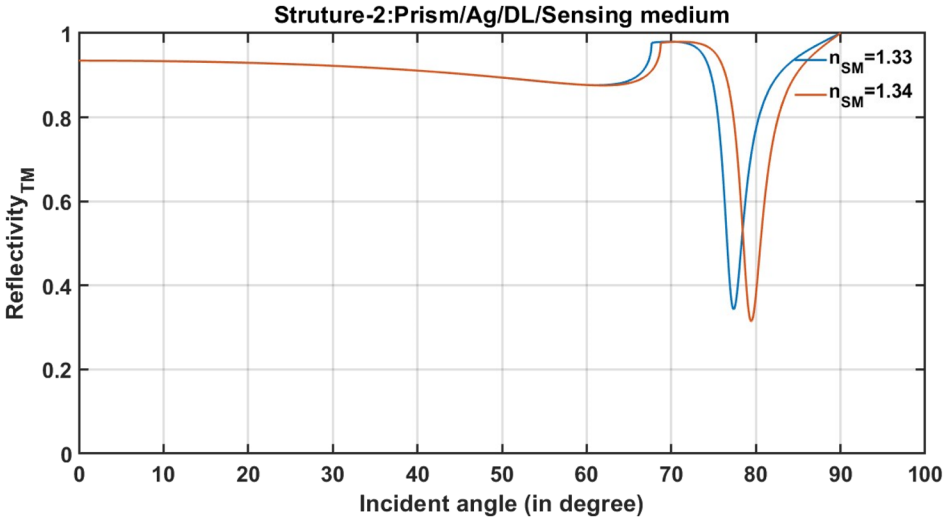

Fig. 3 The incident angle-dependent reflectivity of SPR structure (prism/Ag/DL/sensing medium).

Table 3 The change in the position of the resonant dip ($\Delta\theta_R$ in degrees) is due to a change in the refractive index of the analyte from 1.33 to 1.34 of all structures

Structural details	$\Delta\theta_R$ (°)
Structure-1 (conventional SPR design)	1.92
Structure-2	2.07
Structure-3	2.19
Structure-4	2.10
Structure-5	2.20
Structure-6	1.96
Structure-7	**2.50**

Structure-7 provides large-range surface plasmon resonance (LRSPR). The excitation of LRSPR in multilayer prisms involves a similar process to that of a single-layer metal film. However, in the case of LRSPR, the metal film is sandwiched between two dielectric layers, which alters the resonance conditions and extends the sensing range. The dielectric layers act as waveguides for the surface plasmons, confining them to the metal–dielectric interface and preventing them from decaying into the bulk. This increases the sensor's sensitivity by increasing the interaction time between the surface plasmons and biomolecules. The dielectric layers also affect the coupling of the incident light with the surface plasmons. By choosing the appropriate thickness and refractive index of the dielectric layers, it is possible to match the momentum of the incident light with the momentum of the surface plasmons, leading to enhanced resonance and sensitivity.

LRSPR sensors are designed to have a larger sensing range than the traditional SPR sensors, enabling them to detect the interactions between larger molecules or even whole cells. LRSPR sensors have advanced sensitivity and are capable of detecting sub-nanometer changes in the refractive index. The LRSPR configuration provides a greater electric field penetration depth than the conventional SPR sensors, which can be used to excite a higher number of probe molecules during surface binding events. Unlike traditional SPR sensors, LRSPR sensors have an extended dynamic range, which allows for the detection of both weak and strong binding events. LRSPR sensors are commonly used in drug discovery, medical diagnostics, and environmental monitoring. They can offer high sensitivity, precision, and throughput, making them a valuable tool in the field of biotechnology.

Moreover, using two-dimensional (2D) materials in structure-7 can enhance the sensitivity and specificity of LRSPR sensors by increasing the interaction between the biomolecules and the surface plasmons 1. When incorporated into LRSPR systems, 2D materials can improve surface coverage and reduce background noise, leading to more accurate measurements. Additionally, 2D materials can offer several advantages for sensing, including their high surface area, excellent mechanical properties, and electronic properties that can be tuned by chemical or electrical means.

3.1 The optimization of the 2D material layer used in the architecture of structure-7

This subsection examines the possibility of increasing the shift in the resonant dips further from 2.50° due to the change in the refractive index of the analyte from 1.33 to 1.34 of structure-7. To achieve the objective of this study, the influence of a variety of 2D materials is tested instead of BlueP/WS2 in the architecture of structure-7. The details of 2D materials along with their thicknesses used in this optimization process are illustrated in Table 4.

After selecting different 2D materials in the design of structure-7, the shift in the resonant angle is obtained with the help of reflectance spectra of the respective structures corresponding to the TM polarization case of incident light. The thickness of 2D materials has changed randomly to obtain the maximum shift in the resonant angle associated with each structure. The shift in the resonant angle of each design under the category of structure-7 due to the change in the refractive index of the sample from 1.33 to 1.34 is provided in Table 4, in addition to the 2D material details and their refractive index at λ = 632.8 nm. From this table, it can be concluded that the 2D material tungsten disulfide (WS_2) of thickness 0.80 nm is the best choice for this design. The inclusion of WS_2 material in the proposed design, which belongs to the category of structure-7, increases the shift in the resonant angle from 2.50° to 3.0°. This process helps in identifying the best 2D material WS2 as the most appropriate for the proposed design. Thus, the WS_2 material layer of thickness 0.80 nm has been used as an optimized 2D material layer in the architecture of structure-7, as indicated at the bottom of Table 4.

Tungsten disulfide (WS_2) is a two-dimensional (2D) material, which belongs to the group of transition metal dichalcogenides (TMDs). WS_2 has a layered structure, which consists of one layer of tungsten atoms sandwiched between two layers of sulfur atoms, with van der Waals forces, holding the layers together. WS_2 is studied for its unique properties, making it a promising material for a wide range of applications, including sensing, electronics, and energy storage. In the sensing applications, WS2 is explored for its ability to enhance the sensitivity and specificity of large-range surface plasmon resonance (LRSPR) sensors by improving the surface coverage and reducing the background noise. WS_2 is a direct bandgap semiconductor in the visible range with a high absorption coefficient, making it highly sensitive to changes in the refractive index of the surrounding medium. In addition, WS_2 has a high surface area and excellent mechanical properties, thereby making it ideal for use as a sensing material. Also, the WS_2 has high thermal stability and good mechanical properties, which makes it suitable for use in sensing applications under different environmental conditions.

3.2 Optimization of the dielectric material used in the architecture of structure-7

The selection of the optimized 2D material WS_2 in the architecture of structure-7 has been carried out, as discussed above. To predict the theoretical findings, the investigation started

Table 4 Details of 2D materials used during the optimization of the 2D material layer of structure-7 (ref. 42)

Description of 2D material	Refractive index @ $\lambda = 632.8$ nm	Thickness (nm)	$\Delta\theta$ (°)
Tin selenide (SnSe)	4.4 + 3.53i	1.5	2.06
Graphene oxide (GO)	1.2728 + 0.0039i	2.55	2.13
Titanium disillicide ($TiSi_2$)	2.70008 + 2.9394i	2.00	2.34
Graphene (G)	3.0 + 1.149i	0.35	2.39
Antimonene (Sb)	1.4 + 1.3i	0.50	2.40
2D (BlueP/WS_2)	2.48 + 0.17i	0.57	2.50
Black phosphorus (BP)	3.5 + 0.01i	0.53	2.52
MXene ($Ti_3C_2T_x$)	2.38 + 1.33i	0.993	2.56
Molybdenum diselenide ($MoSe_2$)	4.6226 + 1.0063i	0.70	2.77
Molybdenum disulfide (MoS_2)	5.0805 + 1.1723i	0.65	2.78
Tungsten diselenide (WSe_2)	4.5501 + 0.4332i	0.70	2.79
Tungsten disulfide (WS_2)	**4.8937 + 0.3124i**	**0.80**	**3.02**

with many dielectric materials with refractive indices in the range of 1.5 to 1.91. The thickness of each dielectric layer used in the design is kept at 3.0 nm. The reflectance spectra of structures are simulated with many dielectric materials. The shift in the resonant dips due to the change in the refractive index of the analyte from 1.33 to 1.34 is listed in Table 5. This process helps in optimizing the best dielectric material suitable for high sensitivity. This optimization approach helps in identifying the aluminum oxynitride (AlON) material of refractive index 1.79089 at wavelength 632.8 nm as the most suitable material corresponding to which shift in the resonant dip of the proposed structure-7 due to a change in the refractive index of the analyte from 1.33 to 1.34 that reaches a maximum of 4.23°, which is the best for the proposed design, as illustrated in Table 5. A further change in the dielectric material, whose refractive index increases from 1.79089 results in a decrease in the shift in the resonant dip.

3.3 Evaluation of the performance of optimized structure-7

After the optimization, structure-7, which is composed of prism/Ag/AlON/WS_2/AlON/sensing medium, is ready for the evaluation of the performance in terms of various important performance-evaluating parameters that are associated with any plasmonic and photonics biosensing devices. The next subsection of this study involves the performance evaluation of structure-7 composed of prism/Ag/AlON/WS_2/AlON/sensing medium based on the numeric values of the performance evaluating parameters, as discussed below.

Table 5 Details of dielectric materials used during the optimization of structure-7 (refractive index is shown by alphabet *n*)

Details of dielectric materials	$\Delta\theta$ (°)
n =1.50	2.61
n =1.55	2.81
n =1.60	3.02
Polyimide $n = 1.63795$	3.22
Parylene $n = 1.65848$	3.34
BARLi $n = 1.67537$	3.45
MgO $n = 1.73463$	3.85
Al_2O_3 $n = 1.770$	4.11
AlON $n = 1.79089$	4.23 best
HfO_2 $n = 1.91$	3.37

The reflectance spectra of the optimized structure-7 are shown in Fig. 4. It shows the resonance dips associated with the optimized structure-7 that is composed of prism/Ag/AlON/WS_2/AlON/sensing medium loaded separately with the analytes of the refractive indices 1.330, 1.332, 1.334, 1.336, 1.338, and 1.340.

The performance of the proposed optimized strucutre-7 has been evaluated in terms of sensitivity (S), quality factor (Q), and figure of merit (FoM).[43–45] These are the most common parameters for the evaluation of the performance of all the plasmonic and photonic biosensors. The sensitivity is defined as the ratio of change in the resonant dip due to the corresponding change in the refractive index of the analyte under investigation. It is measured in degrees per RIU as follows:[2–6]

$$S = \frac{\Delta\theta_{SPR}}{\Delta n_S}(\text{degree per RIU}) \quad (5)$$

The ratio of resonant angle (θ_R) with full-width half maximum (FWHM) of the resonant dip is defined as the quality factor of the biosensor. Mathematically it can be defined as follows:[6]

$$Q = \frac{\theta_R}{\text{FWHM} \times R_{min}} \quad (6)$$

The figure of merit of any biosensing device measures how effectively the device can respond due to a minute change in the refractive index of the sample under consideration. It is defined as follows:[3,6]

$$\text{FoM} = \frac{S}{\text{FWHM}} \quad (7)$$

The numeric values of S, Q, and FoM of optimized structure-7 composed of prism/Ag/AlON/WS2/AlON/sensing medium are mentioned in Table 6. For the calibration of these numeric values, the optimized structure-7 has been loaded separately

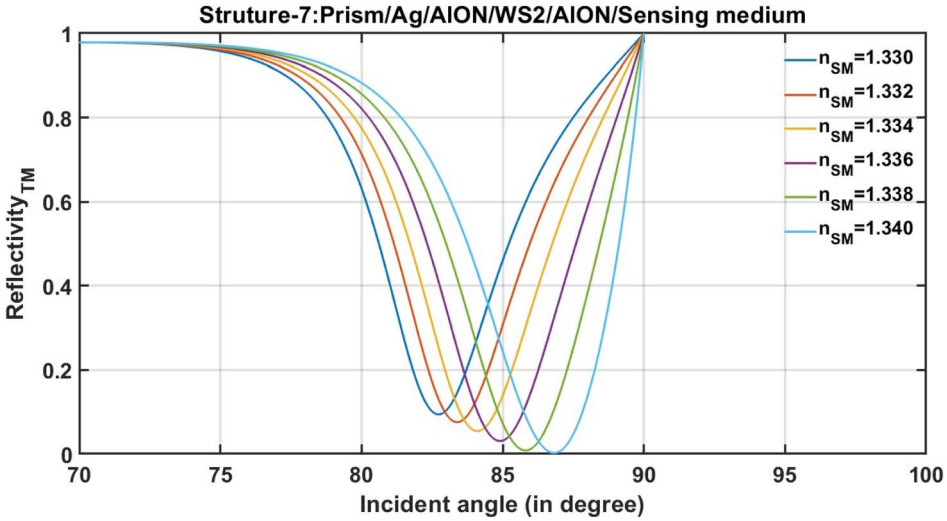

Fig. 4 The incident angle dependent reflectivity of optimized structure-7 that is composed of prism/Ag/AlON/WS_2/AlON/sensing medium loaded separately with the analytes of refractive indices 1.330, 1.332, 1.334, 1.336, 1.338, and 1.340.

with different analytes of refractive indices 1.330, 1.332, 1.334, 1.336, 1.338, and 1.340. The numeric values of the resonant angle, reflectivity, and FWHM of each resonant dip were obtained with the help of the reflectivity plot, as shown previously in Fig. 3.

The notations n_{SM}, θ_R, R, $\Delta\theta_R$, and Δn are used to represent the refractive index of the analyte, resonant angle, and reflectivity of resonant dip at a resonant angle, respectively. Other notations have their usual meaning, as defined above. Based on Table 6, all calibrations were made concerning the analyte of refractive index 1.33 at wavelength 632.8 nm. It can be observed from the analysis of data presented in Table 6 that the proposed MHS, which is composed of prism/Ag/AlON/WS_2/AlON/sensing medium, is a better alternative for sensing and detecting the sample whose refractive index varies from 1.33 to 1.34 in steps of 0.002. It can be observed that the increase in the refractive index of the analyte from 1.330 to 1.340 in steps of 0.002 results in an increase in the resonant angle from 82.977° to 87.203°. Thus, the change in the sensitivity of the structure reached a maximum of 452.3° per RIU. Moreover, at this stage, the FoM and Q values of the optimized design reached 82.93178 per RIU and 15.98 per RIU, respectively. Consequently, in the light of the data presented in Table 6, it can be concluded that the performance of the proposed MHS composed of Prism/Ag/AlON/WS_2/AlON/Sensing medium is better than the contemporary designs as previously reported in ref. 5, 46–48.

Furthermore, the dependency of resonant angle θ_R on the refractive index of the sensing medium of MHS has been examined. To accomplish the objective of the study, Fig. 5 is plotted to show the change in the resonant angle due to the change in the refractive index of the analyte poured into the surface of the sensing medium of the optimized structure composed of prism/Ag/AlON/WS_2/AlON/sensing medium. As can be seen in Fig. 5, the refractive index of the sensing medium increased from 1.330 to 1.340 in steps of 0.002, the resonant angle also increased from 82.977° and finally reached 87.203°, as shown in Table 6 and Fig. 3. Based on Fig. 5, the green color solid balls represent the simulated data, and the black color dashed line represents the linear curve fitting, which is applied to the simulated data, showing n_{SM} dependent discrete values of θ_R. After applying the linear curve-fitting on the theoretical data obtained from MATLAB simulations, the following linear fitting equation is obtained, as given in eqn (8)

$$\theta_R = 423.14\, n_{SM} - 479.9 \quad (8)$$

Here, R^2 is the root mean square value, which is unity in this case as desired.

Table 6 Evaluation of the performance of the optimized structure-7

n_{SM}	θ_R (°)	R_{min}	FWHM	$\Delta\theta_R$ (°)	Δn	S (° per RIU)	FoM (RIU^{-1})	Q
1.330	82.977	0.0838	5.482	—	—	—	—	180.6
1.332	83.656	0.0659	5.505	0.9765	0.002	488.2	88.68888	230.6
1.334	84.407	0.0456	5.492	1.7275	0.004	431.8	78.63453	377
1.336	85.250	0.0241	5.447	2.5703	0.006	428.3	78.63231	649.4
1.338	86.205	0.0061	5.413	3.5256	0.008	440.7	81.40624	2610.7
1.340	87.203	0.0188	5.453	4.226	0.01	452.3	82.93178	850.6

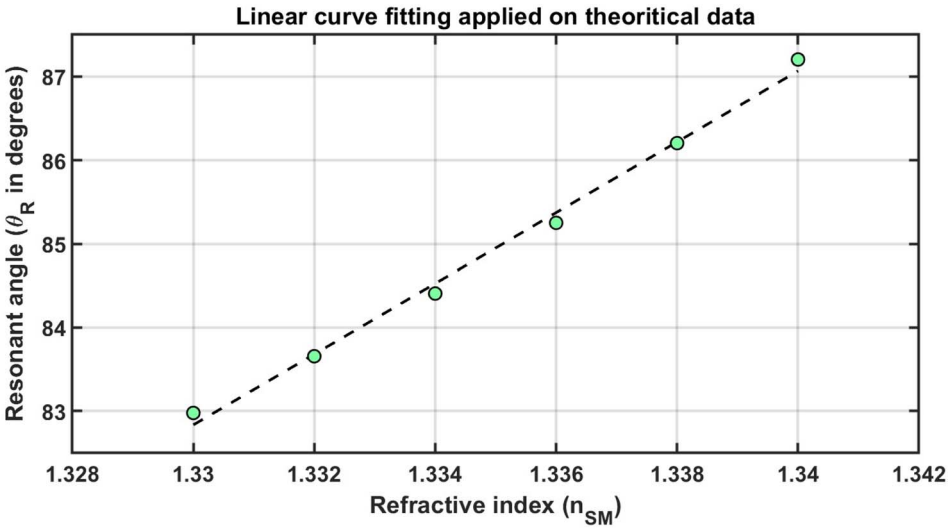

Fig. 5 Linear curve fitting shown by dashed black color line and green color solid balls, showing refractive index dependent resonant angle values.

Moreover, Fig. 5 is used to calculate the numeric values of the limit of detection (LoD) and limit of qualification (LoQ), as defined in the following expressions (9) and (10), respectively.[49]

$$\text{LoD} = \frac{3 \times \text{standard deviation}}{\text{slope}} \quad (9)$$

Then,

$$\text{LoQ} = \frac{10 \times \text{standard deviation}}{\text{slope}} \quad (10)$$

Here, the slope of the line is 423.13, as seen from eqn (8) and the standard deviation is 0.018197, as obtained by using the MATLAB data statistics tool of MATLAB figure window, which can be used for obtaining the numeric values of LoD and LoQ of the proposed structure as 0.000142 and 0.00043, respectively.

3.4 Comparison with other sensors based on ASPR

In this subsection, we emphasize the comparative analysis of our numerical results with those of previous sensors relying on surface plasmon resonance (SPR). The incorporation of 2D materials in ASPR sensors has garnered considerable attention, attributed to the pivotal role these materials play in enhancing sensor performance. Interestingly, the dependence of some materials like Graphene, MXene, black phosphorous, blue phosphorous and tungsten disulfide have significant effect on the sensitivity, FoM, quality factor and LoD as well.[2–6,8,10–13] Meanwhile, Yupapin *et al.*, have introduced an ASPR sensor based on Si-Graphene layers for the detection of Chikungunya virus.[3] The suggested sensor provides a sensitivity of 393° per RIU. Also, Srivastava *et al.*, have considered a SPR gas sensor based on a doped graphene monolayer.[4] However, their design investigated a little sensitivity of 40.6° per RIU. On the other hand, the FoM of their sensing tool increased to 741 per RIU. Almawgani *et al.*, have introduced a new theoretical approach for chemical sensing based on ASPR comprising black Phosphorous and Al_2O_3.[6] Interestingly, the proposed design could provide a relative high sensitivity and quality factor of 466° per RIU and 2252 per RIU, respectively. For instance, a combination of ZnO, Au, MoS_2 and graphene was considered by Angad *et al.* to design an ASPR sensor with a sensitivity of 101.58° per RIU.[50] Also, Xu *et al.* demonstrated a sensitivity of 131.70° per RIU based on the inclusion of tungsten disulfide within ASPR sensor *i.e.*, [prism/Au/Si/WS_2].[51] Moreover, Xu *et al.* demonstrated the role of MXene through SPR designs providing a sensitivity of 198° per RIU.[52] In another study, Mohamed *et al.* provided a sensitivity of 205° per RIU based on an ASPR of the configuration, Au–Fe_2O_3–Au.[53] However, the inclusion of two metallic layers leads to a very low FoM value of 17.2407 per RIU resulting in low SPR coupling. Furthermore, Sayed *et al.*, have discussed the detection of water pollution using an ASPR sensor comprising a combination of silver and silver nanocomposite layers.[54] Meanwhile, the designed structure have obtained a relatively high sensitivity of 448° per RIU. However, the considered design could collide with some obstacles during the manufacturing process. Notably, the investigated value of the sensitivity is strongly dependent on the volume fraction of silver nanoparticles through the nanocomposite layer. To sum up, our design could be of a significant interest through the sensing and detection of chemical and biomedical components of refractive index in the range from 1.33 to 1.34 compared with its counterparts. In particular, our design provides a higher performance response in the vicinity of sensitivity, quality factor and FoM compared with its counterparts as listed in Table 7. In this regard, our design is specified with sensitivity, FoM, and quality factor of 488.2° per RIU, 88.69 per RIU and 2610.7, respectively. In addition, the proposed design is characterized by the simplicity and ease during the experimental verifications.

Table 7 Comparison between the sensitivity of our designed structure with recent ASPR sensors

The designed structure	Sensitivity (° per RIU)	Q	Reference
SPR biosensor based on Si-graphene layers for the detection of chikungunya virus	393	Not mentioned	3
SPR based gas sensor using doped graphene monolayer and organic material	40.6	Not mentioned	4
ASPR chemical sensor based on black phosphorous and aluminum oxide	466	2252.6	6
SPR biosensor comprising zinc oxide, MoS_2 and graphene	101.58	15.11	50
Long range SPR biosensor based on Si and tungsten disulfide	131.7	Not mentioned	51
SPR liquid sensor based on MXene, tungsten disulfide and transition metal dichalcogenide	198	Not mentioned	52
SPR biosensor comprising Fe_2O_3 layer coupled with Au thin film	205.4	676.8	53
ASPR for water pollution detection based on silver nanocomposite and $BiFeO_3$	448.1	20.03	54
SPR biosensor for fat concentration detection in milk employing Si and MXene	350	Not mentioned	55
SPR sensor for blood plasma detection based on sheets of black phosphorus	124	Not mentioned	56
SPR biosensor based on Ni/ZnO nanocomposite and graphene layers	378.34	39.78	57
SPR biosensor comprising aluminum oxynitride and tungsten disulfide	**488.2**	**2610.7**	Our current study

3.5 Experimental setup

The multilayer hybrid biosensor prism/Ag/AlON/WS_2/AlON/sensing medium can be easily fabricated on the surface of the Ohara S-FPL53 prism by adopting the following steps. First, the surface of the Ohara S-FPL53 prism must be cleaned with methanol, vapors of acetone along with some deionized water. High-quality silver layer depositing on prism by using the atomic layer deposition (ALD) technique at a lower temperature.[58] Next, an ultra-thin layer of aluminum oxynitride (AlON) is deposited on the top of the prism/Ag structure by using the ALD method. ALD offers atomic-scale precision, meaning it can deposit films with high accuracy down to the atomic level. Hence, ALD is an exact thin film deposition technique that offers several advantages.[59] ALD allows for the deposition of thin films with excellent film quality, precise composition control, contamination-free deposition, good adhesion, and precise control of the thickness. Moreover, the thin film layers produced *via* ALD display smooth surfaces and demonstrate consistency in both thickness and composition. These films are devoid of cracks, defects, and columnar growth.[60] Additionally, ALD films offer atomic-scale precision, conferring several benefits such as the ability to finely tailor interfaces. This precision proves advantageous in diverse applications. For instance, in semiconductor devices, meticulous control over interfaces between distinct materials can augment device performance and functionality. ALD is a versatile technique that can be used to deposit a wide variety of materials, including metals, oxides, nitrides, and sulfides. It serves different applications of various fields such as solar cell fabrication, optical coatings, biomedical devices, and microelectronics. After that, the chemical vapor deposition (CVD) technique in a vacuum is used to grow an extremely fine layer of 2D material WS_2 on the top of the structure prism/Ag/AlON.[61] CVD refers to the deposition of a film on a solid substrate by the chemical reaction of a gas. A characteristic feature of the CVD technique includes excellent throwing power, selective deposition, uniform coating of rough surfaces, low vacuum requirements, and superior adhesion at low temperatures. Also, it can generate highly pure and dense films or particles. These advantages make CVD a versatile and desirable technique for various industrial applications. Finally, one additional layer of AlON is fabricated on the top of the structure prism/Ag/AlON/WS_2 for the protraction of the WS_2 material layer by using ALD. After completing the fabrication of a multilayer hybrid structure in the form of a single chip, it is connected through other experimental equipment so that monochromatic polarized light can be injected from the He–Ne laser into the structure *via* prism to detect the intensity of the reflected light with the help of a photodetector to evaluate performance.

There are many previous experimental works reported for sensors based on angular interrogation of SPR. Yafeng *et al.* developed an SPR sensor for the detection of nucleic acid hybridization.[62] The sensor was made by fabricating a gold film modified with bovine serum albumin (BSA). The SPR system used a prism with a refractive index of 1.72 and a flow cell module in the traditional Kretschmann prism configuration. The sensitivity of this sensor structure was measured at 3.72×10^{-6} RIU. Chii-Wann *et al.* successfully fabricated an SPR sensor based on an alternating dielectric multi-layer for the detection of glucose solutions.[63] The sensor has a symmetrical construction made of a prism/Au/$(SiO2/TiO2)^4$/Au/sensing medium. The SPR sensor has a practical sensitivity of 75.617° per RIU for detecting glucose concentrations in the weight percentage range of 10% to 40%. Sajal *et al.* conducted a study on the fabrication and characterization of an SPR sensor utilizing a titanium/silver thin film on indium tin oxide (ITO) coated glass.[64] The metal layer was fabricated using the vacuum evaporation-deposition method. The structural characterization of the sensor was performed using atomic force microscopy (AFM) and X-ray diffraction (XRD). The refractive index of the sensor was measured to be between 1.39 and 1.41. The experimental results demonstrated a sensitivity of approximately 300° per RIU for the ITO/Ti/Ag sensor. Kaijie *et al.* investigated an angular SPR sensor with optimal angle-pixel resolution for detecting human immunoglobulin *G* (IgG).[65] The sensor used a Kretschmann-type sensing setup, with a ZF6 prism/Cr/Au/MgF_2 structure. The structures were fabricated using magnetron sputtering and vacuum evaporation techniques. The sensor's pixel sensitivity was determined by measuring the shift of the resonance angle with a CCD camera pixel. The sensor has

a linear response to IgG concentration with a sensitivity of 34.22 pixel (μg^{-1} mL^{-1}). Shigeru *et al.* used a waveguide-coupled prism device as an SPR sensor.[66] The waveguide structure was created by progressively depositing thin Ag, SiO_2, and Au films on a prism. The proposed structure (prism/Ag/SiO_2/Au) was created utilizing electron beam vapor deposition and an RF-sputtering system. Experimental data from both P- and S-waves revealed a sharp absorption characteristic in the light reflectance curve. These absorptions are caused by the surface plasmon resonance phenomena and the attenuation of light traveling through the waveguide due to repetitive absorption at the metal/SiO_2 boundary, respectively.

The presented study suggests that the sensor comprises a prism (Ohara S-FPL53)/Ag/AlON/WS_2/AlON/sensing medium. The sensitivity of the proposed sensor is 452.3° per RIU for detecting analytes with refractive index variations limited between 1.33 and 1.34. This result is competitive, considering the simplicity of the film structure and the economical nature of the sensor system. Using 2D materials improve the proposed structure due to their unique optical and electrical properties. Also, the of LRSPR configuration enhance the evanescent wave which result in strong SPR. The proposed sensor presents numerous benefits, such as excellent performance, effective selectivity, straightforward fabrication, and cost-effectiveness. These attributes render it highly promising for potential commercial applications across various fields. Moreover, the findings of this study could offer valuable insights for improving and optimizing other angular plasmonic sensors.

3.6 Selectivity and performance for different gases and biomolecules

Conducting computations for various biomolecules and gas molecules is undertaken to analyze the sensor's effectiveness and appraise its capabilities. When it comes to gases, their refractive indices are acknowledged to be close to one under atmospheric pressure owing to their low density. Specifically, the refractive index values for helium, neon, hydrogen, oxygen, argon, air, nitrogen, and carbon dioxide are approximately 1.000036, 1.000066, 1.000139, 1.000272, 1.000281, 1.000293, 1.000297, and 1.000448, respectively. If a gas sample were used as the sensing medium in the proposed structure instead of a liquid sensing medium, the sensitivity was found to be approximately 68.44° per RIU. This sensitivity value is obtained when the refractive index of the gas sample changed from 1.000036 to 1.000448 as shown in Fig. S1 in the ESI.†

Using our optimized structure, we calculated the sensitivity of several biomolecules, including cholesterol, urea, glucose, and protein, as shown in Table 8 and Fig. S1 in the ESI.†. When the concentration of cholesterol changes from 0.2 to 4.0 mg mL^{-1}, the corresponding refractive index changes from 1.000036 to 1.000448. The sensitivity for cholesterol is calculated to be 174.64° per RIU, which is equivalent to 0.712° (mg^{-1} mL^{-1}). The sensitivity values for glucose, urea, and protein are 369.735, 207.793, and 178.551° per RIU, respectively. The related figure of each gas and biomolecule is plotted and inserted in the ESI (Fig. S1†).

4. Conclusion

In this work, an innovative method of designing an optimized multilayer hybrid biosensing structure is introduced. The proposed design is composed of Ohara S-FPL53 prism, silver, AlON, and 2D tungsten disulfide. The sensing medium has been kept on the top of the structure, so that the analyte under investigation can be poured on the surface of the sensing medium of the design. Ten dielectrics and twelve 2D materials were tested to find the most suitable dielectric, as well as 2D materials for the proposed design, so that the sensing and detection capabilities of the design achieve the maximum performance. Apart from testing these materials, an investigation has been carried out to examine a total of six structures related to the conventional SPR structures to find the most optimum biosensing design. Finally, the most suitable and high-performing design is obtained, which is composed of Ohara S-FPL53 prism/Ag/AlON/WS_2/AlON/sensing medium. This design is capable of sensing the analyte whose refractive index variation is limited between 1.330 and 1.340. The highest sensitivity achieved by this design is about 452.3° per RIU with FoM and Q values of 82.93178 and 15.98, respectively. The LoD and LoQ values of the proposed structure are 0.000142 and 0.00043, respectively. Finally, the future perspectives and challenges of this type of a sensor design concentrated in obtaining a high efficient design with acceptable agreement between the experimental and simulation results. Therefore, the study of the effects of tolerance, roughness and topological optimization are crucial parameters could enhance and produce a stable and efficient design of angular SPR biosensors. Additional, some new techniques that rely on the use of binder materials on the surface of this biosensor are a promising idea as well. These methods could represent a novel and forward-thinking strategy to elevate the biosensor's performance, as the binder materials establish connections and interactions with biomolecules, providing insights into their structure and ultimately improving sensor functionality.

Table 8 The selectivity and sensitivity of our designed structure for different biomolecules and gas molecules

	Equation	Concentration changes	S
Gas			68.44° per RIU
Cholesterol	$n = 1.33257 + 0.00408C$ (ref. 67)	0.2 to 4.0 mg mL^{-1}	174.619° per RIU = 0.712° (g^{-1} mL^{-1})
Glucose	$n = 1.33\,230\,545 + 0.00011889C$ (ref. 68)	0 to 5 g L^{-1}	369.753° per RIU = 0.039° (g^{-1} L^{-1})
Urea	$n = 1.3331 + 0.1455C$ (ref. 69)	0 to 0.1 g g^{-1}	207.793° per RIU = 30.234° (g^{-1} g^{-1})
Protein	$n = 1.3384 + 1.5985 \times 10^{-3}C + 3.1 \times 10^{-5}$ C^2 (ref. 70)	0 to 4% (kg kg^{-1})	178.551° per RIU = 0.290° (kg^{-1} kg^{-1})

Ethical statement

I, hereby, the corresponding author declare that the authors have thoroughly read the Journal Policy and admitted all its requirements. Specially, I declare here that this contribution is original and has not been published anywhere. I also declare that this article doesn't contain any plagiarized materials. No part of this manuscript has been introduced in any conference or published in any journal.

Data availability

The data that support the findings of this study will be made available from the corresponding author upon reasonable request.

Author contributions

A. M. Ahmed and H. A. Elsayed conceived of the presented idea and developed the theory. A. M. Ahmed, A. H. M. Almawgani, Y. A. A. Ali and H. A. Elsayed. A. Mehaney performed the computations. S. Kumar Awasthi wrote the manuscript with support from H. A. Elsayed, A. Mehaney and A. H. M. Almawgani, S. Kumar Awasthi, Y. A. A. Ali, A Alzahrani and A. H. M. Almawgani visualization, administration, and funding. All authors discussed the results and contributed to the final manuscript.

Conflicts of interest

The authors declare they have no conflicts of interests.

Acknowledgements

The authors are thankful to the Deanship of Scientific Research and the supervision of the Scientific and Engineering Research Centre at Najran University for funding this work under the Research centers funding program grant code (NU/RCP/SERC/12/4).

References

1 B. Liedberg, C. Nylander and I. Lunström, Surface plasmon resonance for gas detection and biosensing, *Sens. Actuators*, 1983, **4**, 299–304.
2 R. C. Jorgenson and S. S. Yee, A fiber-optic chemical sensor based on surface plasmon resonance, *Sens. Actuators, B*, 1993, **12**, 213–220.
3 P. Yupapin, Y. Trabelsi, D. Vigneswaran, S. A. Taya, M. G. Daher and I. Colak, Ultra-high-sensitive sensor based on surface plasmon resonance structure having Si and graphene layers for the detection of chikungunya virus, *Plasmonics*, 2022, **17**, 1315–1321.
4 T. Srivastava, A. Purkayastha and R. Jha, Graphene based surface plasmon resonance gas sensor for terahertz, *Opt. Quant. Electron.*, 2016, **48**, 1–11.
5 R. Shivangani, P. Lohia, P. K. Singh, S. Singh and D. K. Dwivedi, Design and modeling of reconfigurable surface plasmon resonance refractive index sensor using Al_2O_3, nickel, and heterostructure blueP/WSe2 nanofilms, *J. Opt.*, 2022, 1–12.
6 A. H. Almawgani, S. K. Awasthi, A. Mehaney, G. A. Ali, H. A. Elsayed, H. Sayed and A. M. Ahmed, A theoretical approach for a new design of an ultrasensitive angular plasmonic chemical sensor using black phosphorus and aluminum oxide architecture, *RSC Adv.*, 2023, **13**, 16154–16164.
7 J. Kim, S. Hong and Y. Choi, Sensitive detection of formaldehyde gas using modified dandelion-like SiO_2/Au film and surface plasmon resonance system, *J. Nanosci. Nanotechnol.*, 2019, **19**, 4807–4811.
8 M. G. Daher, Y. Trabelsi, N. M. Ahmed, Y. K. Prajapati, V. Sorathiya, S. H. Ahammad and A. N. Z. Rashed, Detection of basal cancer cells using photodetector based on a novel surface plasmon resonance nanostructure employing perovskite layer with an ultra-high sensitivity, *Plasmonics*, 2022, **17**, 2365–2373.
9 S. A. Maier, *Plasmonics: Fundamentals and Applications*, Springer, New York, vol. 1, 2007, p. 245.
10 F. A. Alzahrani and V. Sorathiya, Phase change material and MXene composited refractive index sensor for a wide range of sensing applications at visible and infrared wavelength spectrum, *Optik*, 2023, **272**, 170242.
11 L. Wu, K. Che, Y. Xiang and Y. Qin, Enhancement of sensitivity with high– reflective– index guided– wave nanomaterials for a long– range surface plasmon resonance sensor, *Nanomaterials*, 2022, **12**, 168.
12 A. Uniyal, B. Chauhan, A. Pal and Y. Singh, Surface plasmon biosensor based on Bi_2 Te_3 antimonene heterostructure for the detection of cancer cells, *Appl. Opt.*, 2022, **61**, 3711–3719.
13 B. Karki, A. Uniyal, G. Srivastava and A. Pal, Black phosphorous and cytop nanofilm-based long-range SPR sensor with enhanced quality factor, *J. Sens.*, 2023.
14 M. M. Rahman, M. M. Rana, M. S. Rahman, M. S. Anower, M. A. Mollah and A. K. Paul, Sensitivity enhancement of SPR biosensors employing heterostructure of PtSe2 and 2D materials, *Opt. Mater.*, 2020, **107**, 110123.
15 S. N. Nangare and P. O. Patil, Affinity-based nanoarchitectured biotransducer for sensitivity enhancement of surface plasmon resonance sensors for *in vitro* diagnosis: a review, *ACS Biomater. Sci. Eng.*, 2020, **7**, 2–30.
16 S. A. Taya, N. E. Al-Ashi, O. M. Ramahi, I. Colak and I. S. Amiri, Surface plasmon resonance-based optical sensor using a thin layer of plasma, *JOSA B*, 2021, **38**, 2362–2367.
17 J. Homola and M. Piliarik, *Surface Plasmon Resonance (SPR) Sensors*, Springer Berlin Heidelberg, 2006, pp. 45–67.
18 V. Chabot, Y. Miron, M. Grandbois and P. G. Charette, Long range surface plasmon resonance for increased sensitivity in living cell biosensing through greater probing depth, *Sens. Actuators B*, 2012, **174**, 94–101.
19 D. Sarid, *et al.*, Long-range surface-plasma waves on very thin metal films, *Phys. Rev. Lett.*, 1981, **47**, 1927.

20 D. Hou, X. Ji, N. Luan, L. Song, Y. Hu, M. Luo and J. Liu, Surface plasmon resonance sensor based on double-sided polished microstructured optical fiber with hollow core, *IEEE Photon. J.*, 2021, **13**, 1–8.
21 A. W. Wark, H. J. Lee and R. M. Corn, Long-range surface plasmon resonance imaging for bioaffinity sensors, *Anal. Chem.*, 2005, **77**, 3904–3907.
22 P. S. Pandey, Y. Singh and S. K. Raghuwanshi, Theoretical analysis of the LRSPR sensor with enhance FOM for low refractive index detection using MXene and fluorinated graphene, *IEEE Sens. J.*, 1981, **21**, 23979–23986.
23 A. Uniyal, A. Pal and B. Chauhan, Long-range SPR sensor employing platinum diselenide and cytop nanolayers giving improved performance, *Phys. B*, 2023, **649**, 414487.
24 P. H. Chang, C. Lin, N. Engheta and A. S. Helmy, Tailoring of modal losses in anisotropic 2D material ribbons by regulating material absorption, *JOSA B*, 2020, **37**, 3681–3689.
25 A. Srivastava and Y. K. Prajapati, Performance analysis of silicon and blue phosphorene/MoS 2 hetero-structure based SPR sensor, *Photon. Sens.*, 2019, **9**, 284–292.
26 A. Sinha, H. Zhao, Y. Huang, X. Lu, J. Chen and R. Jain, MXene: an emerging material for sensing and biosensing, *TrAC, Trends Anal. Chem.*, 2018, **105**, 424–435.
27 Ashour M. Ahmed and Ahmed Mehaney, Ultra-high sensitive 1D porous silicon photonic crystal sensor based on the coupling of tamm/fano resonances in the mid-infrared region, *Sci. Rep.*, 2019, **9**, 6973.
28 L. Fu, M. Lin, Z. Liang, Q. Wang, Y. Zheng and Z. Ouyang, The transmission properties of one-dimensional photonic crystals with gradient materials, *Materials*, 2022, **15**, 8049.
29 A. M. Ahmed and A. Mehaney, Novel design of wide temperature ranges sensor based on Tamm state in a pyroelectric photonic crystal with high sensitivity, *Phys. E*, 2021, **125**, 114387.
30 L. Aarik, H. Mandar, P. Ritslaid, A. Tarre, J. Kozlova and J. Aarik, Low-temperature atomic layer deposition of α-Al_2O_3 thin films, *Cryst. Growth Des.*, 2021, **21**, 4220–4229.
31 Z. Chai, Y. Liu, J. Li, X. Lu and D. He, Ultra-thin Al_2O_3 films grown by atomic layer deposition for corrosion protection of copper, *RSC Adv.*, 2014, **4**, 50503–50509.
32 J. B. Smith, D. Hagaman and H. F. Ji, Growth of 2D black phosphorus film from chemical vapor deposition, *Nanotechnology*, 2016, **27**, 215602.
33 S. K. Awasthi, U. Malaviya and S. P. Ojha, Enhancement of omnidirectional total-reflection wavelength range by using one-dimensional ternary photonic bandgap material, *JOSA B*, 2006, **23**, 2566–2571.
34 M. Upadhyay, S. Awasthi, S. Srivastava and S. Ojha, Infrared omni-directional mirror based on one-dimensional birefringent-dielectric photonic crystal, *Prog. Electromagn. Res. M*, 2012, **25**, 211–222.
35 Z. S. Matar, M. Al-Dossari, S. K. Awasthi, D. Mohamed, N. S. Abd El-Gawaad and A. H. Aly, Conventional biophotonic sensing approach for sensing and detection of normal and infected samples containing different blood components, *Crystals*, 2022, **12**, 650.
36 C. Malek, M. Al-Dossari, S. K. Awasthi, Z. S. Matar, N. S. Abd El-Gawaad, W. Sabra and A. H. Aly, Employing the defective photonic crystal composed of nanocomposite superconducting material in detection of cancerous brain tumors biosensor: computational study, *Crystals*, 2022, **12**, 540.
37 A. H. Aly, S. K. Awasthi, D. Mohamed, Z. S. Matar, M. Al-Dossari and A. F. Amin, Study on a one-dimensional defective photonic crystal suitable for organic compound sensing applications, *RSC Adv.*, 2021, **11**, 32973–32980.
38 N. Kumari, A. D. Varshney, S. K. Awasthi, L. Shiveshwari and A. H. Aly, Polarization-dependent zero-plasma-permittivity, zero-permittivity, and zero-permeability gaps in a 1D photonic crystal composed of lossy double-negative and magnetic cold plasma materials, *JOSA B*, 2022, **39**, 2341–2355.
39 *Refractive Index of Ohara S-FPL53 for Thin Film Thickness Measurement*, **https://www.filmetrics.com/**.
40 P. B. Johnson and R. W. Christy, Optical constants of the noble metals, *Phys. Rev. B: Condens. Matter Mater. Phys.*, 1972, **6**, 4370.
41 Q. Peng, Z. Wang, B. Sa, B. Wu and Z. Sun, Electronic structures and enhanced optical properties of blue phosphorene/transition metal dichalcogenides van der Waals heterostructures, *Sci. Rep.*, 2016, **6**, 1–10.
42 *Refractive Index Database – Table of Refractive Index Values for Thin Film Thickness Measurement*, **https://www.filmetrics.com/**.
43 M. Al-Dossari, Z. A. Zaky, S. K. Awasthi, H. A. Amer and A. H. Aly, Detection of glucose concentrations in urine based on coupling of Tamm–Fano resonance in photonic crystals, *Opt. Quant. Electron.*, 2023, **55**, 484.
44 C. Malek, S. A. O. Abdallah, S. K. Awasthi, M. A. Ismail, W. Sabra and A. H. Aly, Biophotonic sensor for swift detection of malignant brain tissues by using nanocomposite $YBa_2Cu_3O_7$/dielectric material as a 1D defective photonic crystal, *Sci. Rep.*, 2023, **13**, 8115.
45 C. Malek, M. Al-Dossari, S. K. Awasthi, M. A. Ismail, N. A. El-Gawaad, W. Sabra and A. H. Aly, High performance biosensor composed of 1D defective photonic crystal for sensing and detection of distinguished blood components, *Opt. Quant. Electron.*, 2023, **55**, 196.
46 Shivangani, M. F. Alotaibi, Y. Al-Hadeethi, P. Lohia, S. Singh, D. K. Dwivedi and S. Baskoutas, Numerical study to enhance the sensitivity of a surface plasmon resonance sensor with BlueP/WS2-covered Al_2O_3-nickel nanofilms, *Nanomaterials*, 2022, **12**, 2205.
47 A. H. Almawgani, M. G. Daher, S. A. Taya, M. M. Olaimat, A. R. Alhawari and I. Colak, Detection of blood plasma concentration theoretically using SPR-based biosensor employing black phosphor layers and different metals, *Plasmonics*, 2022, **17**, 1751–1764.
48 A. H. Almawgani, M. G. Daher, S. A. Taya, M. Mashagbeh and I. Colak, Optical detection of fat concentration in milk using MXene-based surface plasmon resonance structure, *Biosensors*, 2022, **12**, 535.

49 R. Saad, A. Gamal, M. Zayed, A. M. Ahmed, M. Shaban, Mohammad BinSabt, Mohamed Rabia and Hany Hamdy, Fabrication of ZnO/CNTs for application in CO_2 sensor at room temperature, *Nanomaterials*, 2021, **11**, 3087.
50 A. S. Kushwaha, A. Kumar, R. Kumar and S. K. Srivastava, *Photon. Nanostruct. Fundam. Appl.*, 2018, **31**, 99–106.
51 Y. Xu, C. Y. Hsieh, L. Wu and L. K. Ang, *J. Phys. D Appl. Phys.*, 2019, **52**, 065101.
52 Y. Xu, Y. S. Ang, L. Wu and L. K. Ang, *Nanomaterials*, 2019, **9**(2), 165.
53 A. M. Ahmed and M. Shaban, Highly sensitive Au–Fe_2O_3–Au and Fe_2O_3–Au–Fe_2O_3 biosensors utilizing strong surface plasmon resonance, *Appl. Phys. B*, 2020, **126**, 57.
54 F. A. Sayed, H. A. Elsayed, M. Al-Dossari, *et al.*, Angular surface plasmon resonance-based sensor with a silver nanocomposite layer for effective water pollution detection, *Sci. Rep.*, 2023, **13**, 21793.
55 A. H. Almawgani, M. G. Daher, S. A. Taya, M. Mashagbeh and I. Colak, Optical detection of fat concentration in milk using MXene-based surface plasmon resonance structure, *Biosensors*, 2022, **12**, 535.
56 A. H. Almawgani, M. G. Daher, S. A. Taya, M. M. Olaimat, A. R. Alhawari and I. &Colak, Detection of blood plasma concentration theoretically using SPR-based biosensor employing black phosphor layers and different metals, *Plasmonics*, 2022, **17**, 1751–1764.
57 P. Maheswari, S. Subanya, A. Nisha, *et al.*, Sensitivity enhancement of SPR sensor using Ni/ZnO nanocomposite assisted with graphene, *Opt. Quant. Electron.*, 2021, **53**, 727.
58 Y. I. Xu, L. Wu and L. K. Ang, Highly sensitive near-infrared surface plasmon resonance refractive index sensor, *IEEE J. Select. Top. Quant. Electron.*, 2018, **25**, 1–7.
59 T. Justin Kunene, L. K. Tartibu, K. Ukoba and T.-C. Jen, Review of atomic layer deposition process, application and modeling tools, *Mater. Today Proc.*, 2022, **62**, S95–S109.
60 Z. Chai, Y. Liu, J. Li, X. Lu and D. He, Ultra-thin Al_2O_3 films grown by atomic layer deposition for corrosion protection of copper, *RSC Adv.*, 2014, **4**, 50503–50509.
61 J. B. Smith, D. Hagaman and H. F. Ji, Growth of 2D black phosphorus film from chemical vapor deposition, *Nanotechnology*, 2016, **27**, 215602.
62 Y. Huang, L. Zhang, H. Zhang, Y. Li, L. Liu, Y. Chen, X. Qiu and D. Yu, Development of a portable SPR sensor for nucleic acid detection, *Micromachines*, 2020, **11**, 526, DOI: **10.3390/mi11050526**.
63 C.-W. Lin, K.-P. Chen, C. N. Hsiao, S. Lin and C.-K. Lee, Design and fabrication of an alternating dielectric multi-layer device for surface plasmon resonance sensor, *Sens. Actuators B*, 2006, **113**(1), 169–176.
64 S. Agarwal, P. Giri, Y. K. Prajapati and P. Chakrabarti, Effect of surface roughness on the performance of optical SPR sensor for sucrose detection: fabrication, characterization, and simulation study, *IEEE Sens. J.*, 2016, **16**(24), 8865–8873.
65 K. Ma, L. Liu, P. Zhang, Y. He and Q. Peng, Optimization of angle-pixel resolution for angular plasmonic biosensors, *Sens. Actuators, B*, 2019, **283**, 188–197.
66 S. Toyama, N. Doumae, A. Shoji and Y. Ikariyama, Design and fabrication of a waveguide-coupled prism device for surface plasmon resonance sensor, *Sens. Actuators, B*, 2000, **65**(1–3), 32–34.
67 Y. Luo and J. Luo, Experimental research on cholesterol solution concentration sensing based on tilted fiber Bragg grating, *Optoelectron. Lett.*, 2021, **17**, 661–664.
68 A. H. Aly, Z. A. Zaky, A. , S. Shalaby, A. M. Ahmed and D. Vigneswaran, Theoretical study of hybrid multifunctional one-dimensional photonic crystal as a flexible blood sugar sensor, *Phys. Scr.*, 2020, **95**, 035510.
69 L. Dan-Feng and Q. Zhi-Mei, Glass/Ta_2O_5 composite waveguides for application as an integrated polarimetric interferometer, *Chin. Phys. Lett.*, 2010, **27**(10), 104206.
70 C.-Y. Tan and Y.-X. Huang, Dependence of refractive index on concentration and temperature in electrolyte solution, polar solution, nonpolar solution, and protein solution, *J. Chem. Eng. Data*, 2015, **60**(10), 2827–2833.